Fırat Kafkas
Atakan Uğraş ✉

https://doi.org/10.21278/TOF.482044022
ISSN 1333-1124
eISSN 1849-1391

INVESTIGATING THE EFFECT OF TIG-ASSISTED MACHINING ON THE SPECIFIC CUTTING FORCE, SPECIFIC CUTTING ENERGY AND CHIP SHRINKAGE COEFFICIENT

Summary

Heat-assisted machining is one of the methods used to process moderate to difficult-to-machine materials. Laser, plasma, induction current, oxy-gas flame, and electric current are the primary energy sources used for preheating. In this paper, the Tungsten Inert Gas (TIG) technique is used, which can be considered an alternative and economical energy source for preheating. Both conventional and TIG-assisted machining (TIGAM) experiments in the same cutting conditions are performed and the results are compared. In the TIGAM method, the specific cutting force ($k_{c1.1}$) decreases due to the increase in the work material temperature (T_{mr}). The decrease of $k_{c1.1}$ provides a maximum reduction of specific cutting energy (E_{SC}) of 17.17 %. Thus, plastic deformation of the chip is facilitated, and the chip shrinkage coefficient (λ) decreases. The cutting process is conducted with a high material removal rate (MRR) using a carbide cutting tool using the TIGAM method.

Key words: *heat-assisted machining, specific cutting force, specific cutting energy, chip shrinkage coefficient, TIG*

1. Introduction

It has been known for centuries that heat has a positive effect on the shaping of materials. Due to an increase in temperature, the elastic modulus, yield strength, and tensile strength of materials decrease, while the percentage of elongation increases [1]. Therefore, it is possible to perform plastic deformation with lower forces and higher speeds. This change is valid for many types of materials [2]. Due to heating, the yield strength, hardness, and work hardening tendency of material in the cutting zone decrease. Therefore, the power consumed by the machine tool is also reduced [3], and the chip removal process is achieved with lower cutting forces [4]. Furthermore, in the heat-assisted machining method, the MRR increases [5], tool wear declines [6], the surface quality improves [7], hardened parts can be machined with carbide cutting tools [8], and grinding can be eliminated [9]. Since no coolant is used, there is less environmental damage [10], and machining is performed at higher cutting speeds (V_c) [11]. The heat-assisted machining method is based on the principle of locally heating the workpiece

surface with an energy source and then machining this area with a cutting tool. Using the heat-assisted machining method, different types of energy sources are used for the heating process, such as laser [12], induction current [13], plasma arc [14], oxy-gas flame [15], and electric current [16]. When using an oxy-gas flame for preheating, processed and unprocessed surfaces are affected by the heat [17] because the flame has a wide area of influence. In preheating with an induction current, it is necessary to use special induction coils for the surface to be processed [18, 19]. Machining with electric current is an old technique [20]. Using this technique, the cutting tool performs the task of an electrode [16]. However, the high temperature resulting from the electric arc may cause damage to the cutting tool. Due to the high heat generated by the plasma [3], high temperatures can be reached in the cutting zone. For the plasma technique to be used efficiently, it is necessary to position the torch correctly [7]. It is not as easy to use as a laser. Compared to other techniques, the laser is easier to control. Due to the adjustable spot size [21] and high power [22], it is possible to heat a narrow area. Despite its high cost, these advantages have made the laser a preferred choice.

The TIG technique is another energy source suitable for heat-assisted machining [23]. Compared to other heat sources, the TIG welding machine is easier to access. It is economical, and the maintenance cost is lower than that of laser and plasma. It is suitable for point cutting and can heat a narrow area of work material. In addition, parametric settings (current, shielding gas flow rate, etc.) can easily be made to control the energy input. As in machining with an electric current, the cutting tool is not used as an electrode. A TIG welding machine is suitable for automation applications [24]. The primary disadvantage of the TIG technique is that work materials have electrical conductivity. The specific cutting force ($k_{c1.1}$, N/mm^2) value is used in the calculations of the cutting force (F_c, N) [25]. The $k_{c1.1}$ value represents the cutting force corresponding to the chip section (A, mm^2) of 1x1 mm. This value may differ for each material group (iron alloys, stainless steel, hardened steel, etc.), as may the values for sub-material groups within each group. In this paper, $k_{c1.1}$ was calculated and compared with the literature to determine the advantages of the TIGAM method for cutting. Specific cutting energy (E_{SC}, kJ/cm^3) is the amount of energy consumed by the machine tool to cut a unit volume of material [26]. E_{SC} is an evaluation function for reducing power consumption [27]. The E_{SC} values are known for many materials [26, 28]. These values can be used to calculate the energy consumption required for the cutting process. The energy consumed for preheating means that the TIGAM method consumes more energy than the conventional method. In the TIGAM method, total energy consumption (E_T, kJ/cm^3) to cut a unit volume of chip was determined. E_T is another instrument used to compare the conventional method and the TIGAM method. The chip shrinkage coefficient (λ) can be used to evaluate the performance of the cutting process [29]. λ gives manufacturers an idea about the cutting process and allows the operator to control the machining parameters. The decrease in the λ value indicates that the plastic deformation of the chip is facilitated [30]. There is a relationship between the E_{SC} and λ. As the E_{SC} value decreases, the λ value also falls. In the experiments, the power consumed in the cutting process (P_c, kW), the work material temperature (T_{mr}, ℃), and the power consumed by the TIG welding machine for preheating (P_{TIG}) were measured online. The experiment plan was prepared with the full factorial experiment approach. In this paper, an analysis of variance (ANOVA) and effect charts were used to determine the effect of the process parameters on the results and to determine the interaction between the results. Both conventional and TIGAM experiments were performed in the same cutting conditions. In the experiments, it was observed that $k_{c1.1}$, E_{SC}, and λ decrease due to the TIGAM. In addition, as the MRR increases, E_T decreases in the TIGAM.

2. Material and Method

2.1 Experiment equipment, work material and insert

The experiments were carried out on a universal lathe with a maximum power of 7 kW. An air-cooled TIG welding machine, which can operate at a maximum current of 200 A, was used as the energy source for preheating during the experiments. To use the TIG welding machine at high current values, zirconium alloy 4 mm diameter tungsten electrodes were used. The tip of the tungsten electrode was conically sharpened at an angle of 30° before each machining. A special electrode grinding machine was employed for this. Argon gas was used as a shielding gas at a flow rate of 16 l/min. The study used AISI 4340 steel material, which is a type of steel widely employed in engineering applications. The samples were prepared in diameters of 104-115.5-127 mm to obtain three different cutting speeds (V_c) and hardened to a hardness value of 50 HRC. The chemical composition of the work material and the heat treatment conditions are given in Table 1. As the cutting tool, Sandvik's SNMG 120408-QM 4225 carbide insert with CVD method multi-layer coating (TICN+AL2O3+TIN) and P25 quality was used. A tool holder with the code PSBNR2525M12 with a 75° approach angle (κ) was used for the cutting insert.

Table 1 Chemical composition and the heat treatment process of AISI 4340 steel

Alloy Elements							
C (%)	Si (%)	Mn (%)	P (%)	S (%)	Cr (%)	Mo (%)	Ni (%)
0.41	0.21	0.66	0.011	0.005	0.72	0.21	1.7

Thermal Treatment Process		
Quenching (°C)	Cooling method	Tempering (°C)
850	Oil	370

2.2 Process parameters and experiment plan

Since hardened work material was used in the experiments, the cutting speed (V_c) values were revised at the rate recommended in the catalogue of the cutting tool manufacturer. When the speed of the work material or energy source is increased, the amount of heat entering the work material per unit of time decreases [31]. To increase the heat input, the feed rate (f) values were taken low. The cutting depth (a_p) was taken as a constant 1 mm in the experiments. In the TIGAM experiments, the TIG welding machine was used for preheating at a constant current intensity of 200 A. Table 2 shows the process parameters of the experiments and their levels. The MRR gives researchers an idea about the performance of the cutting process. This value was obtained by multiplying the cutting parameters (V_c, f, a_p). The experiment plan and the MRR values of both the conventional and the TIGAM experiments are given in Table 3.

Table 2 Process parameters and levels

Factor	Unit	Level 1	Level 2	Level 3
Cutting speed (V_c)	m/min	159	176	194
Feed rate (f)	mm/rev	0.11	0.18	0.24
Processing method		Conventional	TIGAM	

2.3 Energy and temperature measurements

PAC2200 model digital display energy meters of the Siemens company were used to determine the power consumed by the lathe, and by the TIG welding machine. A panel was made for the energy meters, and the circuit elements connected to it. The panel of the energy meter system is shown in Figure 1.

Table 3 Experiment plan for the conventional method and TIGAM

Exp. No	V_c(m/min)	f(mm/rev)	MRR (cm^3/min)
1	159	0.11	17.49
2	159	0.18	28.62
3	159	0.24	38.16
4	176	0.11	19.36
5	176	0.18	31.68
6	176	0.24	42.24
7	194	0.11	21.34
8	194	0.18	34.92
9	194	0.24	46.56

Power data were taken once per second with the software of the energy meter, and the measured power data were saved to the computer via an ethernet connection as files with an .xlsx file extension. The power measured on the lathe represents the power consumed by the lathe. Some of this power is spent on mechanical movements such as chuck rotation and automatic feed. When the cutting tool starts to remove chips, additional power is needed other than this power. This refers to the P_c. The P_c was determined from the difference between the power measured after it started cutting and the power measured before it started cutting.

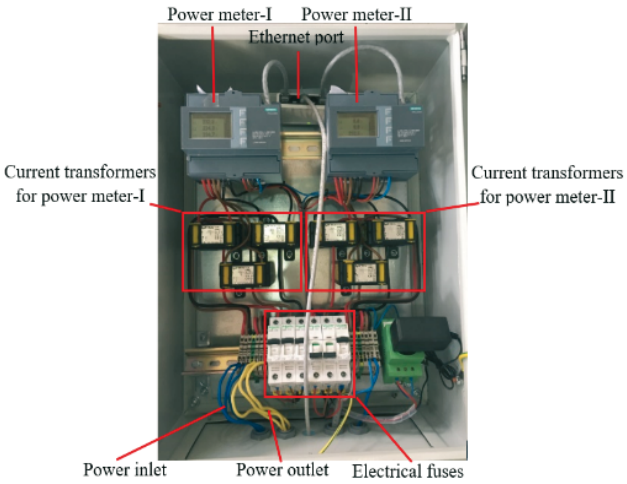

Fig. 1 Energy meter system panel view

Example graphs of the P_c and for power consumption by the lathe are shown in Figure 2(a) and Figure 2(b). If an example is given for calculating P_c, the power consumption read in the energy meter before cutting is 1.98 kW, and after the cutting tool starts cutting the power consumption increases to 3.69 kW. When the difference between the two is taken, P_c is realised as 1.71 kW. P_c is determined by calculating the arithmetic average of the power data in the five-second time period in which the data are stable, and repeating. In Figure 2(a), an immediate increase in power is seen at the beginning. The reason is the resistance to plastic deformation at the start of cutting due to the hardness of the work material. In Figure 2(b), it is seen that the

cutting process becomes more stable [32] because the resistance decreases due to preheating. E_{SC} (kJ/cm^3) was determined using Equation (1). Thus, the change in energy consumption depending on the increase in MRR was evaluated. The total energy consumption (E_T) for the cutting process was calculated by dividing the sum of the power consumed in the cutting process (P_c) and the power consumed by the TIG welding machine for preheating (P_{TIG}) to the MRR, as in Equation (2). In the conventional method, E_{SC} and E_T are equal, because there is no preheating.

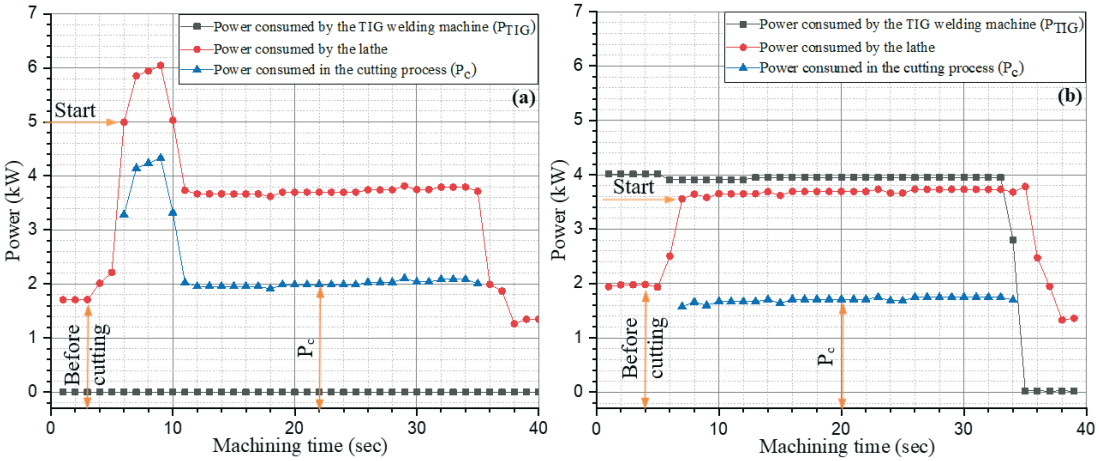

Fig. 2 Power measurements (V=159 m/min, f=0.18 mm/rev) conventional method (a), TIGAM (b)

$$E_{sc} = \frac{P_c}{MRR} \tag{1}$$

$$E_T = \frac{P_C + P_{TIG}}{MRR}\,. \tag{2}$$

As shown in Figure 3, temperature measurement was made from a point on the cutting edge, approximately 9 mm from the cutting zone. The measured temperature is expressed, at the time of cutting, as the work material temperature (T_{mr}). The cutting zone temperature was not measured directly in order to prevent the chip from getting in front of the thermometer and causing measurement errors. A Raytek MI3 infrared thermometer, which can measure temperature in the range of 250-1400 °C, was used to determine the work material temperature (T_{mr}). To go above 250 °C, preheating was done for about 8-10 seconds, at the beginning of the rotating workpiece, and then the cutting was started. Through the original software of the infrared thermometer, 10 pieces of temperature data per second were taken and recorded on the computer. In the determination of the T_{mr}, the path followed in the determination of the P_c was followed, and temperature data corresponding to the same time were used. The position of the cutting tool, the TIG torch, and the infrared thermometer relative to each other is schematically shown in Figure 3, and the experimental setup is given in Figure 4.

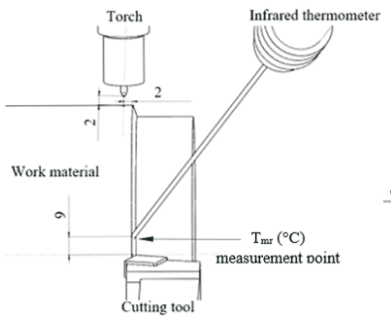

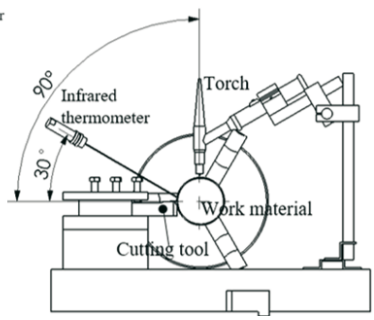

Fig. 3 Schematic view of the TIGAM system

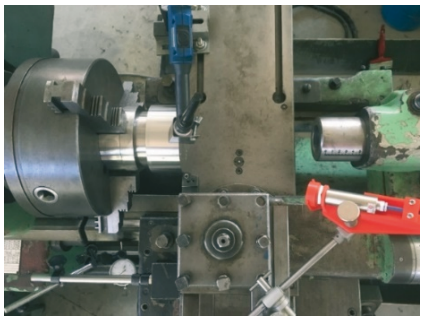

Fig. 4 Experimental setup

2.4 Calculation of the chip shrinkage coefficient (λ)

The chip shrinkage coefficient (λ) was obtained by dividing the cut chip thickness (h_c) by the uncut chip thickness (h) [30]. This ratio is realised as λ>1. To determine the h_c (mm), the thickness of 10 chip samples belonging to each experiment was measured with a digital caliper with a precision of 0.01 mm, and the arithmetic average was taken. When determining the h (mm), the approach angle (κ) of the cutting tool should be taken into account. The κ used in our study is 75°. The h is calculated by Equation (3). After measuring the h_c and calculating the h, λ was calculated by Equation (4):

$$h = f \cdot \sin\kappa \tag{3}$$

$$\lambda = \frac{h_c}{h} \tag{4}$$

2.5 Calculation of specific cutting force ($k_{c1.1}$)

The $k_{c1.1}$ refers to the specific cutting force (N/mm^2) used to cut the chip section (A) with an uncut chip thickness (h) of 1 mm and a width (b) of 1 mm. $k_{c1.1}$ values according to the different hardness values of the work material are given in Table 4. The multiplication of the feed rate (f) and the depth of cut (a_p) can be used for A. However, considering the cutting tool approach angle (κ), it would be more accurate to calculate h with Equation (3) and b with Equation (5) since A is a parallel edge. A can be calculated with Equation (6).

Table 4 $k_{c1.1}$ values for different hardnesses of the work material [33]

Brinell (HB)	Rockwell C (HRC)	$k_{c1.1}$ (N/mm^2)	m
240	≈23	1950	
330	≈35	2000	0.25
475	50	3090	

$$b = \frac{a_p}{\sin\kappa} \tag{5}$$

$$A = h \cdot b \tag{6}$$

As h increases, the cutting resistance of the work material decreases. The increment value (m) is the slope of the curve showing the logarithmic relationship between cutting resistance and chip thickness (h). m takes a fixed value according to the material type. In this paper, the value of 0.25 given in Table 4 determined by the cutting tool manufacturer was taken. While calculating the $k_{c1.1}$ value, first of all the cutting force F_C (N) was calculated with Equation (7) by using the P_c obtained in the experiments. The transformation of Equation (8) to Equation (9) is used to find the value of $k_{c1.1}$.

$$F_c = \frac{P_c \cdot 60000}{V} \tag{7}$$

$$F_c = A \cdot k_{c1.1} \cdot h^{-m} \tag{8}$$

$$k_{c1.1} = \frac{F_c}{A \cdot h^{-m}} \tag{9}$$

3. Experimental Results

Table 5 shows the measured data in the experiments (T_{mr}, P_c, P_{TIG}), and in Table 6 the calculated data (E_{SC}, E_T, λ, $k_{c1.1}$) are given.

Table 5 Data measured in the experiments

Exp. No	T_{mr} (°C)		P_c (kW)		P_{TIG} (kW)
	Conv.	TIGAM	Conv.	TIGAM	TIGAM
1	458	501	1.43	1.22	3.95
2	441	493	1.99	1.71	3.95
3	398	479	2.48	2.09	3.99
4	451	500	1.57	1.37	3.90
5	435	488	2.21	1.87	3.98
6	397	475	2.77	2.31	3.95
7	447	497	1.77	1.47	4.09
8	432	486	2.44	2.06	3.98
9	394	465	3.07	2.54	4.06

The increase in T_{mr} causes the P_c value to decrease. Through the TIGAM, a maximum decrease of 17.17 % was achieved in the E_{SC} value. In the same cutting conditions, lower P_c, E_{SC}, λ, and $k_{c1.1}$ values are obtained in the TIGAM method compared to the conventional method. In the TIGAM method, E_T is higher due to P_{TIG}.

Table 6 Calculated data

Exp. No	E_{SC} (kJ/cm^3)			E_T (kJ/cm^3)		λ		$k_{c1.1}$ (N/mm^2)	
	Conv.	TIGAM	Reduction in E_{SC} (%)	Conv.	TIGAM	Conv.	TIGAM	Conv.	TIGAM
1	4.91	4.19	14.66%	4.91	17.74	1.60	1.56	2801	2390
2	4.17	3.59	13.91%	4.17	11.87	1.48	1.43	2694	2315
3	3.91	3.29	15.86%	3.91	9.56	1.36	1.25	2710	2280
4	4.86	4.24	12.76%	4.86	16.31	1.54	1.52	2773	2423
5	4.18	3.53	15.55%	4.18	11.06	1.46	1.33	2698	2283
6	3.93	3.28	16.54%	3.93	8.88	1.32	1.23	2725	2273
7	4.98	4.14	16.87%	4.98	15.66	1.49	1.42	2846	2364
8	4.19	3.55	15.27%	4.19	10.40	1.44	1.29	2707	2289
9	3.96	3.28	17.17%	3.96	8.52	1.31	1.26	2750	2279

3.1 Material removal temperature (T_{mr}) and power consumed in the cutting process (P_c) results

Figure 5 shows the changes in the T_{mr} values according to the process parameters. Due to the hardness of the work material, the cutting process was carried out with high E_{SC}. If the T_{mr} values of the conventional method are evaluated, it is seen that there is a small decrease in the T_{mr} value as the cutting speed (V_c) increases. This reduction in temperature can be attributed to the higher MRR, which results in more heat being carried away by the chip, and thus less heat being conducted into the workpiece [34]. As the feed rate (f) increases, the heat released is removed with the chip, and therefore the T_{mr} value measured from the work material surface decreases [35]. If the T_{mr} values of the TIGAM method are evaluated, the T_{mr} value decreases as the cutting parameters (V_c, f) increase. As the machining time is shortened, the heat input is reduced. As a natural consequence of the additional heat input provided in the TIGAM method, the T_{mr} value increases.

Figure 6 shows the changes in P_c values according to the process parameters. The physical increases in the MRR value cause an increase in the P_c value. The TIGAM method provides lower P_c values.

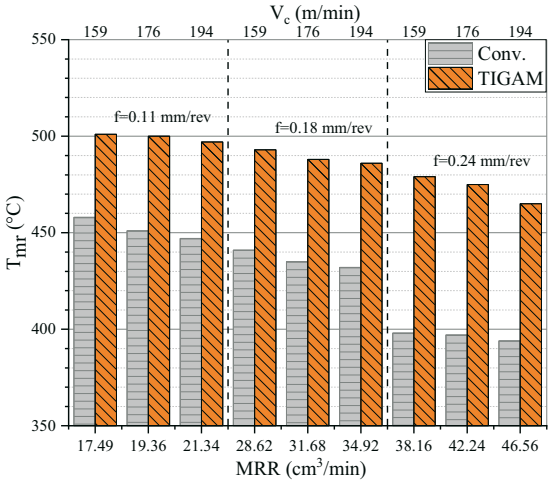

Fig. 5 T_{mr} (°C) values measured in the experiments

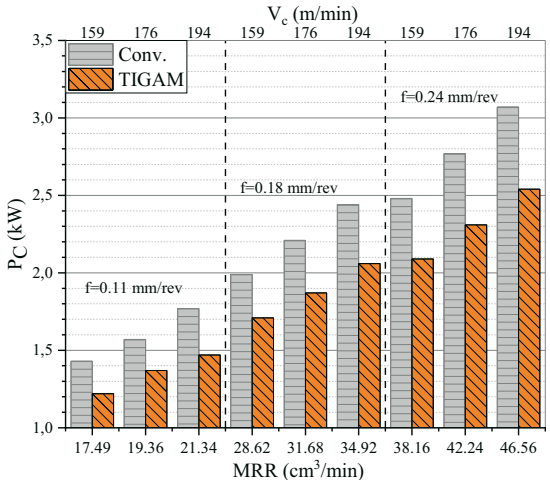

Fig. 6 P_c (kW) values measured in the experiments

3.2 Total energy consumption (E_T) using the TIGAM method

Total energy consumption (E_T) was determined according to Equation (2). When Figure 7 is examined, it is seen that E_T in the TIGAM method is approximately three times higher than the conventional method at the beginning, but this value decreases very quickly as the MRR increases. In the TIGAM method, P_{TIG} remains constant while the P_c changes depending on the cutting parameters. Therefore, E_T decreases as the cutting speed (V_c) and feed rate (f) increase.

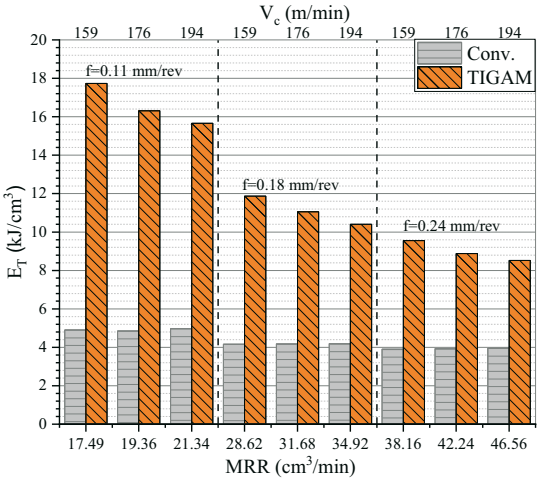

Fig. 7 Variation of the total energy consumption (E_T) depending on the process parameters

3.3 Specific cutting energy (E_{SC}) and chip shrinkage coefficient (λ) results

In the graph given in Figure 8, it is seen that as the MRR value increases, the E_{SC} decreases in both the conventional and the TIGAM methods. Due to the closeness of the cutting speed (V_c) values, there was no significant effect of the cutting speed (V_c) on the E_{SC} value [36]. The decrease in uncut chip thickness (h) due to the decrease in the feed rate (f) causes an increase in the energy consumed due to the phenomenon called "*size effect*" [37]. Therefore, E_{SC} is high at low MRR values. Compared to the conventional method, lower E_{SC} values were obtained in the TIGAM method. The TIGAM method allowed the $k_{c1.1}$ value of the work material to

decrease, so the cutting process was performed with a lower E_{SC}. As the cutting speed (V_c) increases, the cut chip thickness (h_c) decreases. This result is also supported by λ [30]. In Figure 9, it is seen that the increase in the cutting speed (V_c) has an effect on the decrease in λ. The effect of the feed rate (f) on λ is seen the most. As the feed rate (f) increases, the cut chip thickness (h_c) also increases [38]. However, it is not possible to compress the chip at the amount of increase in the feed rate (f), so as the feed rate (f) increases, λ decreases. Figure 9 shows that lower λ values are obtained in the TIGAM method.

High temperatures due to high E_{SC} values cause continuous chip formation in both the conventional method and the TIGAM method. The chip formations (V_c=194 m/min, f=0.24 mm/rev) are shown in Figure 10 and Figure 11. When chip formation and chip-tool contact surfaces are examined, a temper colour is seen in the conventional method, and a metallic colour in the TIGAM method. The metallic color formation shows that the cutting process is facilitated.

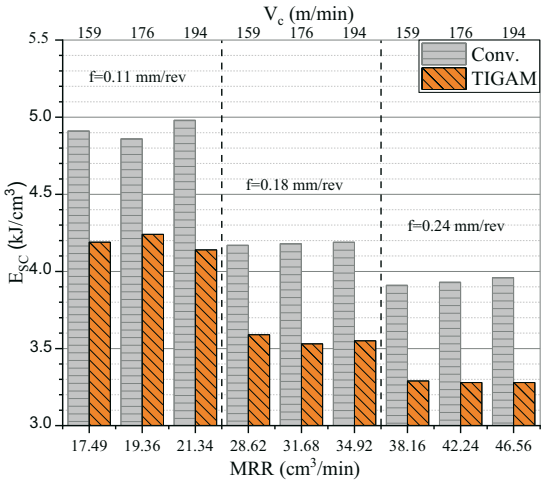

Fig. 8 Variation of specific cutting energy (E_{SC}) depending on the process parameters

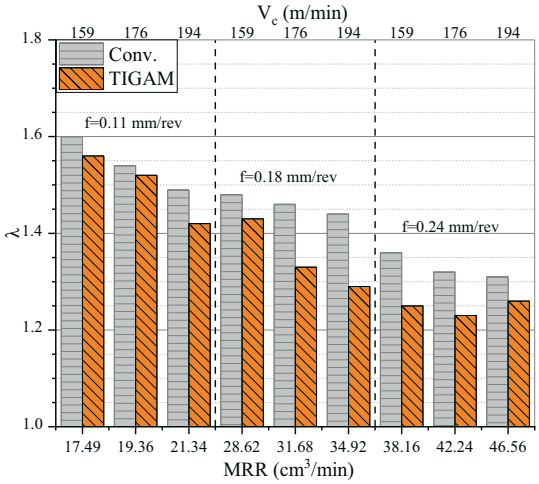

Fig. 9 Variation of λ depending on the process parameter

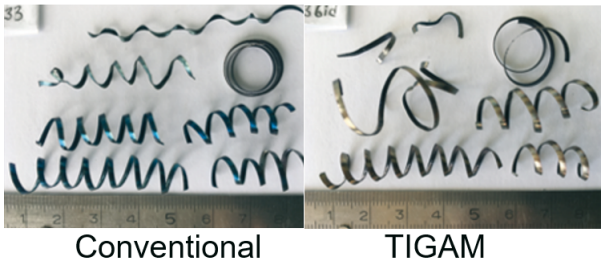

Fig. 10 Chip formation

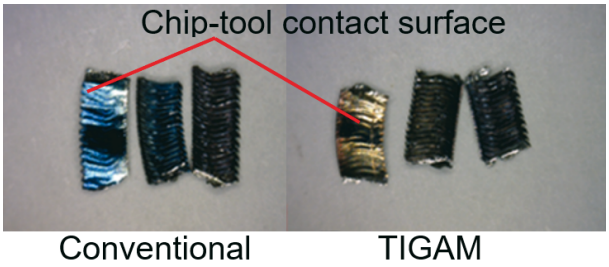

Fig. 11 50x magnified photographs of chips

3.4 Effect of the TIG-assisted machining (TIGAM) method on changes in the specific cutting force ($k_{c1.1}$)

The additional energy spent for preheating reduced the $k_{c1.1}$ (N/mm^2) values. Figure 12 shows the changes in the $k_{c1.1}$ values according to the conventional method and the TIGAM method. It is seen that the $k_{c1.1}$ values calculated for the conventional method are close to the highest value given in Table 4 for the work material, while the values calculated for the TIGAM method are lower. There is no significant change in the $k_{c1.1}$ values depending on the increase in the MRR. Figure 12 shows that the $k_{c1.1}$ is a constant and different value from the E_{SC}.

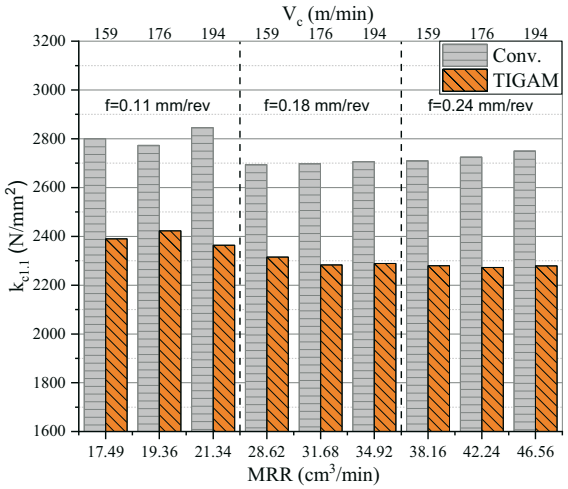

Fig. 12 Variation of the specific cutting force ($k_{c1.1}$) depending on the process parameters

3.5 Analysis of variance (ANOVA) results and effect plots

ANOVA is a statistical approach used to determine the most influential processing parameter on experimental results [39]. The low error rate in the ANOVA tables is an indicator of the accuracy of the findings. Effect graphs are also used to see the effects of the process parameter levels on the results. Tables 7-11 give the ANOVA results showing the effects of the process parameters on T_{mr}, P_c, E_{SC}, λ, and $k_{c1.1}$ respectively. When their effects are examined, it is seen that the one with the least effect is the cutting speed (V_c). In a previous paper, it was seen that the cutting speed (V_c) was the process parameter that had the least effect on the T_{mr} difference in the TIGAM method [40]. As can be seen in Table 7, the processing method was the process parameter that had the most impact (71.43%) on the increase in T_{mr}. The effect graph in Figure 13 shows that the other process parameter affecting the T_{mr} increase is the feed rate (f). In the TIGAM method, the processing time is prolonged at the low feed rate (f), which increases the heat input [40, 41].

Table 7 ANOVA results for the effect of the process parameters on T_{mr} (°C)

Factor	DF	Adj SS	Adj MS	F-Value	P-Value	Contribution
V_c (m/min)	2	196.83	98.42	1.49	0.2640	0.90%
f (mm/rev)	2	5257.60	2628.80	39.83	0.0000	24.05%
Processing method (Conv. /TIGAM)	1	15617.34	15617.34	236.65	0.0000	71.43%
Error	12	791.92	65.99			3.62%
Total	17	21863.69				100.00%

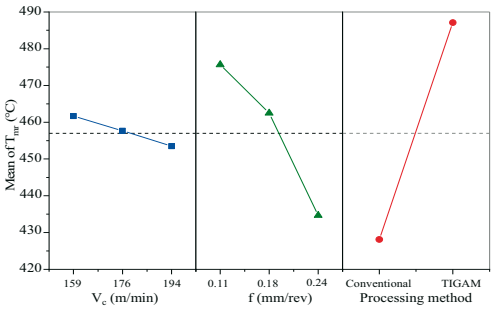

Fig. 13 Main effect plots for T_{mr} (°C)

An increase in the feed rate (f) makes the plastic deformation of the chip more difficult and increases the cutting forces, resulting in higher power consumption. As seen in Table 8, the feed rate (f) is the process parameter with the greatest effect (76%) on P_c. The effect graph in Figure 14 shows that the increase in the cutting speed (V_c) and feed rate (f) increases the P_c value, but the TIGAM method reduces the P_c value. The additional heat input provided by the TIGAM method increases the T_{mr} value, thus lowering the P_c value.

Table 8 ANOVA results for the effect of the process parameters on P_c (kW)

Factor	DF	Adj SS	Adj MS	F-Value	P-Value	Contribution
V_c (m/min)	2	0.49	0.25	40.26	0.0000	10.78%
f (mm/rev)	2	3.46	1.73	283.73	0.0000	76.00%
Processing method (Conv. /TIGAM)	1	0.53	0.53	86.72	0.0000	11.61%
Error	12	0.07	0.01			1.61%
Total	17	4.55				100.00%

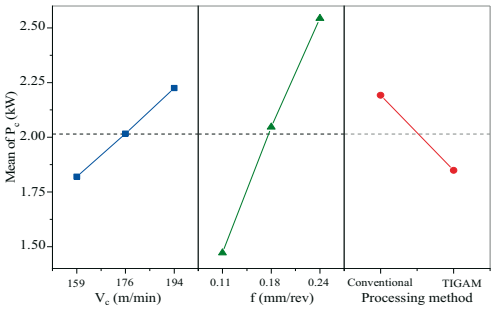

Fig. 14 Main effect plots for P_c (kW)

Table 9 shows that the most effective (58.53%) process parameter on the E_{SC} is the feed rate (f). As stated in Equation (1) above, there is a natural relationship between P_c and E_{SC}. The increase in the feed rate (f) increases the P_c value as well as the E_{SC} value. The effect graph given in Figure 15 displays that the TIGAM method has a significant effect on E_{SC}. In the TIGAM method, the cutting process is carried out with lower E_{SC} values.

Table 9 ANOVA results for the effect of the process parameters on E_{SC} (kJ/cm^3)

Factor	DF	Adj SS	Adj MS	F-Value	P-Value	Contribution
V_c (m/min)	2	0.00	0.00	0.19	0.8282	0.02%
f (mm/rev)	2	2.86	1.43	699.03	0.0000	58.53%
Processing method (Conv. /TIGAM)	1	2.00	2.00	978.05	0.0000	40.95%
Error	12	0.02	0.00			0.50%
Total	17	4.89				100.00%

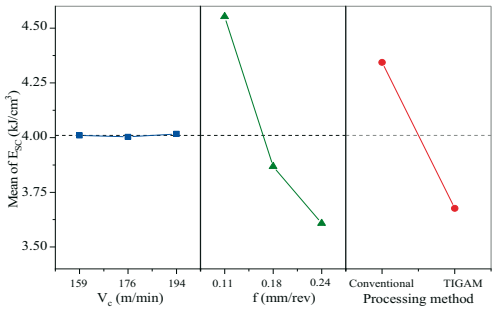

Fig. 15 Main effect plots for E_{SC} (kJ/cm^3)

The most effective process parameter on λ is the feed rate (f) [29]. In Table 10, it is seen that the most effective (73.93%) process parameter on λ is the feed rate (f). When the relationship between the experimental results is investigated, it is seen that λ is related to E_{SC}. The most effective process parameter for both λ and E_{SC} is the feed rate (f). The effect graph given in Figure 16 shows that the increase in the cutting speed (V_c) and the use of the TIGAM method provide a decrease of λ. The increase in cutting speed (V_c) and preheating causes the temperature in the cutting zone to increase. It is considered that this situation causes thinner chip formation and decreases λ.

Table 10 ANOVA results for the effect of the process parameters on λ

Factor	DF	Adj SS	Adj MS	F-Value	P-Value	Contribution
V_c (m/min)	2	0.02	0.01	8.36	0.0053	8.56%
f (mm/rev)	2	0.17	0.08	72.24	0.0000	73.93%
Processing method (Conv. /TIGAM)	1	0.03	0.03	22.23	0.0005	11.37%
Error	12	0.01	0.00			6.14%
Total	17	0.22				100.00%

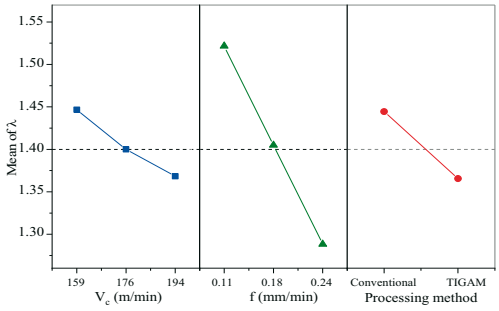

Fig. 16 Main effect plots for λ

The decrease in the $k_{c1.1}$ value in the TIGAM method causes the P_c value to decrease. The ANOVA results in Table 11 indicate that the process parameter that has the most (94.46%) effect on $k_{c1.1}$ is the processing method. This situation also reveals the relationship between $k_{c1.1}$ and T_{mr}. In both, the most effective processing parameter is the processing method. The other process parameter that affects $k_{c1.1}$ is the feed rate (f). However, it can be seen in the effect graph given in Figure 17 that this effect is too low.

Table 11 ANOVA results for the effect of the process parameters on $k_{c1.1}$

Factor	DF	Adj SS	Adj MS	F-Value	P-Value	Contribution
V_c (m/min)	2	334	167	0.27	0.7710	0.04%
f (mm/rev)	2	39364	19682	31.33	0.0000	4.61%
Processing method (Conv. /TIGAM)	1	806086	806086	1283.31	0.0000	94.46%
Error	12	7538	628			0.88%
Total	17	853322				100.00%

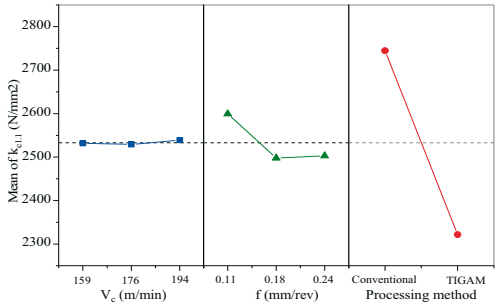

Fig. 17 Main effect plots for $k_{c1.1}$ (N/mm^2)

4. Conclusions

In this paper, AISI 4340 steel material with a hardness of 50 HRC was processed with heat-assisted machining using the TIG technique as the energy source. A CVD-coated carbide cutting tool was used. This study showed that the TIG technique is a suitable energy source for heat-assisted machining. In this regard, the TIG technique is an alternative energy source that can be used for heat-assisted machining, among other energy sources. The results from this research are summarised below:

- In the cutting speed (V_c), both the conventional method and the TIGAM method have almost no effect on the work material temperature (T_{mr}) difference. This situation is due to the use of cutting speed (V_c) values close to each other. Therefore, it was the process parameter that had the least effect on other experimental results.
- The feed rate (f), in both the conventional method and the TIGAM method, is the most effective process parameter in the power consumed in the cutting process (P_c), the specific cutting energy (E_{SC}), and the chip shrinkage coefficient (λ). This describes the relationship between the feed rate (f), the specific cutting energy (E_{SC}), and chip formation.
- In the TIGAM experiments, an increase of up to three times is observed in the total energy consumption (E_T) compared to the conventional method. As the MRR increases, the total energy consumption (E_T) decreases. As the MRR increases, the TIGAM method becomes the more economical method.
- The processing method is the process parameter that has the greatest influence on the T_{mr} and the specific cutting force ($k_{c1.1}$). It also has a very significant effect on E_{SC}.
- The immediate power increase that occurs at the start of cutting in the conventional method does not occur in the TIGAM method. Compared to the conventional method, the cutting process is more stable in the TIGAM method.
- Through the additional heat input provided in the TIGAM method, while the calculated $k_{c1.1}$ value of the work material is a maximum of 2846 N/mm^2 in the conventional method, this value falls to 2364 N/mm^2 in the TIGAM method.
- The E_{SC} value of AISI 4340 steel with a hardness of 50 HRC was determined, between 3.28-4.98 kJ/cm^3 depending on the process parameters. In the TIGAM method, a 17.17% reduction in the E_{SC} value was achieved. Reducing heat losses by optimising the TIGAM method can result in lower E_{SC} values.
- The reduction of E_{SC} in the TIGAM method provides lower λ values.

- Although extra electrical energy is consumed for preheating, not using coolant and cutting with carbide cutting tools are important advantages of the TIGAM method.

REFERENCES

[1] Kalpakjian S, Schmid SR. Manufacturing engineering and technology. (Sixth edition). Pearson Education. 2009. p 64.

[2] Groover MP. Fundamentals of modern manufacturing: materials, processes, and systems. (Fourth edition). John Wiley & Sons. 2010. p 57.

[3] Madhavulu G, Ahmed B. Hot machining process for improved metal removal rates in turning operations. Journal of Materials Processing Technology 1994; 44(3-4): 199-206. https://doi.org/10.1016/0924-0136(94)90432-4

[4] Xavierarockiaraj S, Kuppan P. Investigation of cutting forces, surface roughness and tool wear during laser assisted machining of SKD11 tool steel. Procedia Engineering 2014; 97:1657-1666. https://doi.org/10.1016/j.proeng.2014.12.316

[5] Skvarenina S, Shin YC. Laser-assisted machining of compacted graphite iron. International Journal of Machine tools and Manufacture 2006; 46(1): 7-17. https://doi.org/10.1016/j.ijmachtools.2005.04.013

[6] Dandekar CR, Shin YC, Barnes J. Machinability improvement of titanium alloy (Ti–6Al–4V) via LAM and hybrid machining. International Journal of Machine Tools and Manufacture 2010; 50(2): 174-182. https://doi.org/10.1016/j.ijmachtools.2009.10.013

[7] Moon SH, Lee CM. A study on the machining characteristics using plasma assisted machining of AISI 1045 steel and Inconel 718. International Journal of Mechanical Sciences 2018; 142: 595-602. https://doi.org/10.1016/j.ijmecsci.2018.05.020

[8] Lajis MA, Amin AKMN, Karim ANM, Radzi HCDM, Ginta TL. Hot machining of hardened steels with coated carbide inserts. American Journal of Engineering and Applied Sciences 2009; 2(2): 421-427.

[9] Ding H, Shin YC. Laser-assisted machining of hardened steel parts with surface integrity analysis. International Journal of Machine Tools and Manufacture 2010; 50(1): 106-114. https://doi.org/10.1016/j.ijmachtools.2009.09.001

[10] Shokrani A, Dhokia V, Newman ST. Environmentally conscious machining of difficult-to-machine materials with regard to cutting fluids. International Journal of Machine Tools and Manufacture 2012; 57: 83-101. https://doi.org/10.1016/j.ijmachtools.2012.02.002

[11] Hedberg GK, Shin YC, Xu L. Laser-assisted milling of Ti-6Al-4V with the consideration of surface integrity. The International Journal of Advanced Manufacturing Technology 2015; 79(9): 1645-1658. https://doi.org/10.1007/s00170-015-6942-4

[12] Venkatesan K, Ramanujam R, Kuppan PJPE. Laser assisted machining of difficult to cut materials: research opportunities and future directions-a comprehensive review. Procedia Engineering 2014; 97: 1626-1636. https://doi.org/10.1016/j.proeng.2014.12.313

[13] Kim JH, Kim EJ, Lee CM. A study on the heat affected zone and machining characteristics of difficult-to-cut materials in laser and induction assisted machining. Journal of Manufacturing Processes 2020; 57: 499-508. https://doi.org/10.1016/j.jmapro.2020.07.013

[14] Rao TB. Reliability analysis of the cutting tool in plasma-assisted turning and prediction of machining characteristics. Australian Journal of Mechanical Engineering 2020; 20(10): 1-15. https://doi.org/10.1080/14484846.2020.1769458

[15] Tosun N, Ozler L. Optimisation for hot turning operations with multiple performance characteristics. The International Journal of Advanced Manufacturing Technology 2004; 23(11): 777-782. https://doi.org/10.1007/s00170-003-1672-4

[16] Xu W, Liu X, Sun J, Zhang L. Finite element simulation and experimental research on electric hot machining. The International Journal of Advanced Manufacturing Technology 2013; 66(1): 407-415. https://doi.org/10.1007/s00170-012-4335-5

[17] Davami M, Zadshakoyan M. Investigation of tool temperature and surface quality in hot machining of hard-to-cut materials. World Academy of Science, Engineering and Technology 2008; 2(10): 240-244.

[18] Olsson M, Akujarvi V, Stahl JE, Bushlya V. Cryogenic and hybrid induction-assisted machining strategies as alternatives for conventional method of refractory tungsten and niobium. International Journal of Refractory Metals and Hard Materials 2021; 97:1-14. https://doi.org/10.1016/j.ijrmhm.2021.105520

[19] Choi YH, Lee CM. A study on the machining characteristics of AISI 1045 steel and inconel 718 with circular cone shape in induction assisted machining. Journal of Manufacturing Processes 2018; 34: 463-476. https://doi.org/10.1016/j.jmapro.2018.06.023

[20] Barrow G. The effect of hot machining by electric current on the mechanics of orthogonal cutting. Advances in Machine Tool Design and Research 1967; 2: 795-819.

[21] Garcí V, Arriola I, Gonzalo O, Leunda J. Mechanisms involved in the improvement of Inconel 718 machinability by laser assisted machining. International Journal of Machine Tools and Manufacture 2013; 74: 19-28. https://doi.org/10.1016/j.ijmachtools.2013.06.009

[22] Rashid RR, Sun S, Wang G, Dargusch MS. The effect of laser power on the machinability of the Ti-6Cr-5Mo-5V-4Al beta titanium alloy during laser assisted machining. International Journal of Machine Tools and Manufacture 2012; 63: 41-43. http://dx.doi.org/10.1016/j.ijmachtools.2012.07.006

[23] Amin AKMN, Arif MD, Rasdi NHBM, Mahmud KSB, Ibrahim AHB, Zawani MFB, Malik AFBA. Identification of optimum heating temperature in thermal assisted turning of stainless steel using three different approaches. In Applied Mechanics and Materials 2013; 393: 194-199. https://doi.org/10.4028/www.scientific.net/AMM.393.194

[24] Kapil S, Kulkarni P, Joshi P, Negi S, Karunakaran KP. Retrofitment of a CNC machine for omni-directional tungsten inert gas cladding. Virtual and Physical Prototyping 2019; 14(3): 293-306. https://doi.org/10.1080/17452759.2018.1552484

[25] Karpuschewski B, Kundrak J, Varga G, Deszpoth I, Borysenko D. Determination of specific cutting force components and exponents when applying high feed rates. Procedia CIRP 2018; 77: 30-33. https://doi.org/10.1016/j.procir.2018.08.199

[26] Stephenson DA, Agapiou JS. Metal cutting theory and practice. CRC press. 2018. p 29. https://doi.org/10.1201/9781315373119

[27] Mori M, Fujishima M, Inamasu Y, Oda Y. A study on energy efficiency improvement for machine tools. CIRP Annals 2011; 60(1): 145-148. https://doi.org/10.1016/j.cirp.2011.03.099

[28] Ozerkan HB, Sucularlı, F, Genç, A. The cutting power, specific cutting energy and surface roughness characterization in milling of 8740 steel. Journal of the Faculty of Engineering and Architecture of Gazi University 2022; 37(4): 2057-2066. https://doi.org/10.17341/gazimmfd.948426

[29] Mac TB, Banh TL, Nguyen DT. Study on Cutting Force and Chip Shrinkage Coefficient during Thermal-Assisted Machining by Induction Heating of SKD11 Steel. Journal of the Korean Society for Precision Engineering 2019; 36(9): 803-811. https://doi.org/10.7736/KSPE.2019.36.9.803

[30] Astakhov VP. Tribology of metal cutting. 2006. p 45.

[31] Küçüktürk G, Akıllılar H. Investigating the effect of electron beam melting parameters on the Ti6Al4V alloy: A simulation study. Transactions of FAMENA 2022; 46(4): 45-58. https://doi.org/10.21278/TOF.464038121

[32] Barjašić D, Stegić M, Juran M. Numerical evaluation of plane grinding stability. Transactions of FAMENA 2023; 47(1): 13-20. https://doi.org/10.21278/TOF.471046522

[33] https://www.sandvik.coromant.com/en-us/knowledge/materials/pages/workpiece-materials.aspx (Last accessed: 23 October 2023)

[34] O'Sullivan D, Cotterell M. Temperature measurement in single point turning. Journal of materials processing technology 2001; 118: 301-308. https://doi.org/10.1016/S0924-0136(01)00853-6

[35] Vasudeva, BP, Puneet NP, Akshay Kumar BV. Evaluation of cutting zone temperature in turning of AISI 4340 steel using various tool ınserts. National Conference on Advances in Mechanical Engineering Science 2016; 115-118. https://doi.org/10.1016/j.mspro.2014.07.170

[36] Knight WA, Boothroyd G. Fundamentals of metal machining and machine tools. 2005. p 82.

[37] Davim JP. (Ed.). Modern machining technology: A practical guide. 2011. p 269. https://doi.org/10.1533/9780857094940

[38] Natasha AR, Othman H, Ghani JA, Haron CHC, Syarif J. Chip formation and coefficient of friction in turning S45C medium carbon steel. International Journal of Mechanical and Mechatronics Engineering 2014; 14(6): 89-92.

[39] Mariappan M, Parthasarathi N.L, Ravindran R, Lenin K, Palanisamy A. Improvement of weld bead characteristics in gas metal arc welding of SA515 carbon steel by applying alternating shielding gas flow technique. Transactions of FAMENA 2023; 47(1): 67-85. https://doi.org/10.21278/TOF.471032821

[40] Ugras A, Kafkas F. Applıcability of TIG Technique in Thermal Assist Machining. 10th International On Machining 2019, Antalya, Türkiye.

[41] Kannan MV, Kuppan P, Kumar AS, Kumar KR, Jegaraj JJR. Effect of laser scan speed on surface temperature, cutting forces and tool wear during laser assisted machining of alumina. Procedia Engineering 2014; 97: 1647-1656. https://doi.org/10.1016/j.proeng.2014.12.315

Submitted: 02.07.2022

Accepted: 31.10.2023

Fırat Kafkas
Gazi University, Faculty of Technology, Department of Manufacturing Engineering, 06500, Ankara, Turkey
Atakan Uğraş*
Eskisehir Technical University, Porsuk Vocational High School, Machines and Metal Technologies, 26140, Eskisehir, Turkey
*Corresponding author:
atakanugras@eskisehir.edu.tr